Journal of Power Sources 195 (2010) 6389–6397

Contents lists available at ScienceDirect

Journal of Power Sources

journal homepage: www.elsevier.com/locate/jpowsour

Thermal properties of phosphoric acid-doped polybenzimidazole membranes in water and methanol–water mixtures

Federico J. Nores-Pondal[a,b], M. Pilar Buera[b,c], Horacio R. Corti[a,b,*]

[a] Grupo de Pilas de Combustible, Departamento de Física de la Materia Condensada, Centro Atómico Constituyentes, Comisión Nacional de Energía Atómica (CNEA), Av. General Paz 1499, B1650KNA San Martín, Buenos Aires, Argentina
[b] Consejo Nacional de Investigaciones Científicas y Técnicas, Argentina
[c] Departamento de Industrias, Facultad de Ciencias Exactas y Naturales, Universidad de Buenos Aires, Av. Cantilo s/n, Ciudad Universitaria, (1428) Buenos Aires, Argentina

ARTICLE INFO

Article history:
Received 5 February 2010
Received in revised form 3 April 2010
Accepted 5 April 2010
Available online 10 April 2010

Keywords:
PBI
ABPBI
Thermal properties
Phosphoric acid
Water
Fuel cells

ABSTRACT

The thermal properties of phosphoric acid-doped poly[2-2′-(m-phenylene)-5-5′ bi-benzimidazole] (PBI) and poly[2,5-benzimidazole] (ABPBI) membranes, ionomeric materials with promising properties to be used as electrolytes in direct methanol and in high temperature polymer electrolyte membrane (PEM) fuel cells, were studied by means of differential scanning calorimetry (DSC) technique in the temperature range from −145 °C to 200 °C. The DSC scans of samples equilibrated in water at different relative humidities (RH) and in liquid water–methanol mixtures were analyzed in relation to glass transition, water crystallization/melting and solvent desorption in different temperature regions. The thermal relaxation observed in the very low temperature region could be ascribed to the glass transition of the H_3PO_4–H_2O mixture confined in the polymeric matrix. After cooling the samples up to −145 °C, frozen water was detected in PBI and ABPBI at different RH, although at 100% RH less amount of water had crystallized than that observed in Nafion membranes under the same conditions. Even more important is the fact that the freezing degree of water is much lower in ABPBI membranes equilibrated in liquid water–methanol mixtures than that observed for PBI and, in a previous study, for Nafion. Thus, apart from other well known properties, acid-doped ABPBI emerges as an excellent ionomer for applications in direct methanol fuel cells working in cold environments.

1. Introduction

Polymer electrolyte membrane fuel cells (PEMFCs) are one of the promising alternative energy resource systems that can be utilized in many applications such as electric vehicles, portable devices and on-site power generators [1–7].

Recent progress has focused on the need to develop PEMFCs that operate above 100 °C [8,9]. Operation at high temperatures allows the exploitation of many system's design and operation advantages, i.e. no need for humidification, increased kinetic reaction rate, reduced temperature dependent catalyst poisoning from CO, easier and efficient heat management and system integration. Unfortunately, the proton conductivity of Nafion® membrane, which is widely used now in H_2/O_2 and direct methanol (DM) PEMFCs, suffer greatly at temperatures above 80 °C due to the dehydration of the membrane. Indeed, Nafion® membranes have high methanol permeability that diminishes cell efficiency in DM PEMFCs.

The design and synthesis of novel high temperature anhydrous polymer electrolytes constitute the main prerequisite for the successful implementation of High Temperature Proton Exchange Membrane Fuel Cells (HT-PEMFC). The existing state of the art technology is based on materials that combine acid–base interactions [3,4,10] in order to acquire high proton conductivity (>5.10^{-2} S cm^{-1}) at temperatures ranging between 150 °C and 200 °C.

Polybenzimidazoles (PBI) are one of the classes of aromatic heterocyclic polymers known for many years [11], synthesized from aromatic di- or tetraamines and difunctional aromatic acids. One of the members of this family, commonly known as PBI is based on the polymerization of 3,3′-diaminobenzidine and isophthalic acid.

As an electrolyte in fuel cells, PBI needs to be doped with acids, typically phosphoric acid. Strong acid–polymer interaction by way of hydrogen bonding leads to homogeneous systems and ionic conduction occur over the Brønsted acid–base pairs [12]. PBI is amorphous with a glass transition temperature at 420 °C and exhibits high thermal stability, even when it is doped [13], high water and acid uptake, high ionic conductivity [1,14–18], and low

* Corresponding author at: Grupo de Pilas de Combustible, Departamento de Física de la Materia Condensada, Centro Atómico Constituyentes, Comisión Nacional de Energía Atómica (CNEA), Av. General Paz 1499, B1650KNA San Martín, Buenos Aires, Argentina. Tel.: +54 11 6772 7174; fax: +54 11 6772 7121.
E-mail address: hrcorti@cnea.gov.ar (H.R. Corti).

0378-7753/$ – see front matter © 2010 Elsevier B.V. All rights reserved.
doi:10.1016/j.jpowsour.2010.04.009

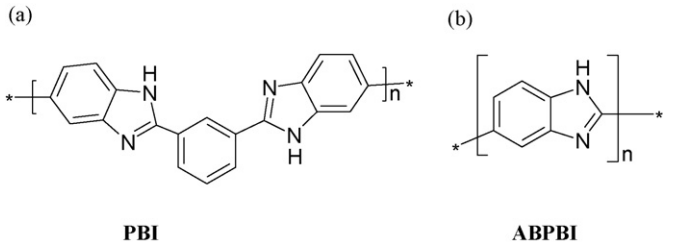

Fig. 1. Structure of PBI (a) and ABPBI (b).

methanol crossover [1,19]. Unlike Nafion®-based protonic conductors, PBI + H_3PO_4 electrolytes achieve a high electrical conductivity even under operation temperatures above 100 °C.

The first high temperature PEMFC based on a PBI membrane with phosphoric acid as an ionic conductor, was proposed by Wainright et al. [1] and has shown to produce good power density at elevated temperatures [20]. Since then, PBI has been thoroughly tested as polymer electrolyte in HT PEM fuel cells [10,21,22].

A number of modified PBI polymers were also studied, including sulfonation of the polybenzimidazole [23–25] and the chemical modification of the monomer unit of the polybenzimidazole polymers [26–31]. One of the simplest polymerization processes to obtain a modified PBI was described by Asensio and Gómez-Romero [28], who synthesized ABPBI, whose chemical structure, along with that of PBI is shown in Fig. 1. We have recently reported the properties of the ABPBI membranes, such as phosphoric acid and water uptake [32], mechanical properties [33], and we compared them with PBI and Nafion® membranes.

The thermal stability of PBI has been extensively studied by thermogravimetric analysis (TGA) with mass spectrometry (MS) [13,34,35] and by differential scanning calorimeter (DSC) [36,37]. Thermal stability of phosphoric acid-doped ABPBI by TGA was reported by Gomez-Romero et al. [38]. They found similar weight losses, at the same temperatures, than the phosphoric acid-doped PBI. In these works, all thermal characterizations of ABPBI and PBI were made at room temperature and above. For acid-doped PBI, typically about 10–15% weight loss occurs at temperatures up to 150 °C, due to absorbed water. There is a second loss starting at 150 °C due to phosphoric acid. The dehydration of phosphoric acid leads to the formation of pyrophosphoric acid, and conductivity drops. From 210 °C to 500 °C, there is no further significant weight loss. At temperatures over 500 °C, a second dehydration of the acid is observed and then polymer decomposes, accompanied by a significant weight loss and carbon dioxide formation.

It is well known that phosphoric acid-doped ABPBI and PBI are very hygroscopic [39] and, under operating PEMFC or DM PEMFC conditions, water is produced in the cathode. At temperatures below 0 °C water that is present in the membrane may crystallize affecting ionic conduction, concerning mainly the start up procedure. This occurs in the case of Nafion® membrane, as it was described in our previous work [40]. Nafion® equilibrated at different RH and methanol–water solutions, presented a high percentage of frozen water, up to 65 wt%, at temperatures lower than −10 °C.

As far as we know, no study has been carried out on the low temperature thermal properties of doped ABPBI and PBI. In this work a systematic study is presented on the thermal properties of phosphoric acid-doped ABPBI and PBI membranes, with different RH and methanol–water solutions, in the temperature range from −145 °C to 200 °C, by means of DSC technique. Analysis is focused in the thermal transitions that undergo the whole system; i.e. polymer matrix, phosphoric acid and water or methanol–water; in relation to its application in PEMFCs. The results will be compared with those obtained for Nafion® 117 under the same conditions [40].

Table 1
Doping degree (λ_a), water sorption (λ_w), and water sorption by mole of phosphoric acid (λ_{wa}) for ABPBI and PBI membranes doped in 10.64 M aqueous H_3PO_4 [32].

Membrane	M_w (g mol^{-1})	λ_a	λ_w	λ_{wa}
PBI	19,600	1.9	2.19	1.0
LT-ABPBI	18,800	3.5	3.35	1.4
HT-ABPBI	18,800	2.8	2.19	0.8

2. Experimental

2.1. Membrane preparation

PBI (Fig. 1a) membranes were prepared from 5 wt% solutions of the commercial powder (Goodfellow) dissolved in N,N-dimethylacetamide (DMA) at 70 °C under stirring. The solution was poured in a glass mould and put in a vacuum furnace at 80 °C during 4 h in order to cast a membrane of thickness ranging from 50 μm to 150 μm.

ABPBI (Fig. 1b) was prepared by condensation of 3,4-diaminobenzoic acid (DABA) monomer in polyphosphoric acid (PPA) following the procedure reported by Asensio and Gómez-Romero [28]. The resulting polymer was condensed in water, grinded, and washed with water. Then it was immersed in stirred aqueous 10 wt% NaOH during 20 h in order to eliminate remaining polyphosphoric acid and then washed until neutral pH was attained. Finally it was dried at 90 °C.

ABPBI membranes were prepared by two casting methods: high temperature (HT-ABPBI) and low temperature (LT-ABPBI) casting, as described elsewhere [32]. Briefly, the HT-ABPBI membranes were casted from a 5 wt% solution of ABPBI in pure methanesulfonic at about 200 °C, while the LT-ABPBI membranes were casted from a 1 wt% solution in formic acid at room temperature.

As prepared membranes were cut into discs of 5 mm and immersed in 10.64 M H_3PO_4 solution in order to protonate the imidazole rings. After three days of equilibration, membranes were removed from the phosphoric acid solution, wiped gently with paper to remove superficial solution and equilibrated at different relative humidities (RH) or, alternatively, immersed in water or methanol–water solutions. Dry membranes (0% RH) were obtained by equilibration with P_2O_5 during several days. When necessary, before DSC experiments, membranes were wiped again to remove excess solution.

2.2. Membrane properties

Water uptake of PBI and ABPBI membranes, measured previously [32], expressed by means of λ_w and λ_{wa}, the number of water molecules per imidazole ring and per mole of acid, respectively, and the degree of acid doping, λ_a, the moles of acid per imidazole ring, are summarized in Table 1. These results correspond to membranes doped in 10.64 M aqueous H_3PO_4 and in isopiestic equilibrium with the same acid solution ($a_w \approx 0.32$). Only a small fraction of the total uptaken acid, about 10%, is not bounded to polymer imidazole groups in the PBI and ABPBI membranes.

The acid doping levels of the PBI and ABPBI membranes are similar to those reported in the literature, except for the case of the PBI membranes prepared by the sol–gel method by casting in polyphosphoric acid (PPA) [18], which exhibit much higher phosphoric acid level.

The water sorption isotherm of PBI and ABPBI doped membranes, determined at 30 °C in the relative humidity range from 0.15 to 1 have the form of type III in the Brunauer classification, for LT-ABPBI and HT-ABPBI membranes, and are type II-like for PBI membranes [32]. It is also observed that at water activity higher than 0.2 the water uptake by ABPBI membranes is higher than in PBI

Table 2
Calculated values of water uptake of ABPBI and PBI doped membranes, expressed as grams of water per gram of dry polymer (m) and mass fraction of water (w_1), and the mass fraction of acid (w_2).[a].

% RH	PBI			LT-ABPBI			HT-ABPBI		
	m	w_1	w_2	m	w_1	w_2	m	w_1	w_2
32	0.28	0.11	0.51	0.52	0.12	0.66	0.34	0.09	0.64
44	0.34	0.13	0.49	0.78	0.16	0.62	0.58	0.15	0.60
84	0.66	0.22	0.44	2.16	0.35	0.48	1.85	0.35	0.45
97	0.86	0.27	0.41	2.92	0.42	0.43	2.73	0.45	0.39
100	0.93	0.29	0.40	3.20	0.45	0.41	3.00	0.47	0.37

[a] The mass fraction of polymer can be obtained as $w_3 = 1 - w_1 - w_2$.

membranes, and LT-ABPBI membranes have higher water uptake than the HT-ABPBI membranes, which is also consistent with the higher acid doping level in the LT-ABPBI membranes. Water sorption of the doped PBI and ABPBI membranes is much higher than the corresponding to Nafion® membranes in its protonated form.

In order to obtain the water uptake at the relative humidities studied in this work: 44, 84, 97 and 100%, we used the Guggenheim–Anderson–de Boer (GAB) equation [41–43] with the parameters obtained from the corresponding isotherms [32]. The calculated water uptakes, expressed as grams of water per gram of dry membrane (m) are shown in Table 2.

The glass transition temperatures (T_g), the reversible change of specific heat capacity at the glass transition (ΔC_p), crystallization and melting temperatures (T_c and T_m, respectively) and heats of crystallization (ΔH_c) and melting (ΔH_m) were determined by DSC using a Mettler 822 and STARe Thermal Analysis System version 6.1 software (Mettler Toledo AG, Switzerland).

Glass transitions were recorded as the onset temperature of the discontinuities in the curves of heat-flow versus temperature (change in heat capacity); crystallization and melting temperatures were taken to be the peak temperatures of the exothermic and endothermic changes, respectively. The instrument was calibrated using standard compounds (indium, zinc and lead) of defined melting point and heat of melting.

All measurements were made with 8–20 mg sample mass, at a scanning rate of 10 °C min^{-1}, using hermetically sealed stainless steel pans, with sputtered gold coating, of 120 μL inner volume (Mettler) and an empty pan was used as a reference. Each sample was cooled and maintained isothermal at −145 °C during 3 min previously to the dynamic DSC runs performed from −145 °C to 200 °C at a scanning rate of 10 °C min^{-1}. Reported data are the average of three determinations.

3. Results and discussion

3.1. Thermal properties of H_3PO_4-doped ABPBI and PBI equilibrated with water

DSC thermograms up to 200 °C of H_3PO_4-doped ABPBI and PBI membranes previously equilibrated at RH values 0, 44, 84, 97 and 100%, are shown in Fig. 2 (note the differences in the y-axis scale). Other thermal events occurring above 200 °C, such as the dehydration of phosphoric acid to pyrophosphoric acid [14] were not considered to be relevant for the purpose of this study.

The observed thermal relaxations will be analyzed separately, namely, the very low temperature region (−140 °C < T < −70 °C), where glass–rubber like transition is observed, the subzero/room temperature region (−70 °C < T < 40 °C), where water melting and crystallization take place, and the water desorption region for the upper temperatures (40 °C < T < 200 °C). We will start discussing the desorption region, where the thermal events are quite clear in the full scale DSC scans, while the weaker transitions in the former two regions require the magnification of the thermograms.

3.1.1. Water desorption

The temperatures corresponding to the endothermic peaks of water desorption, ranged from 105 °C to 150 °C, as can be seen

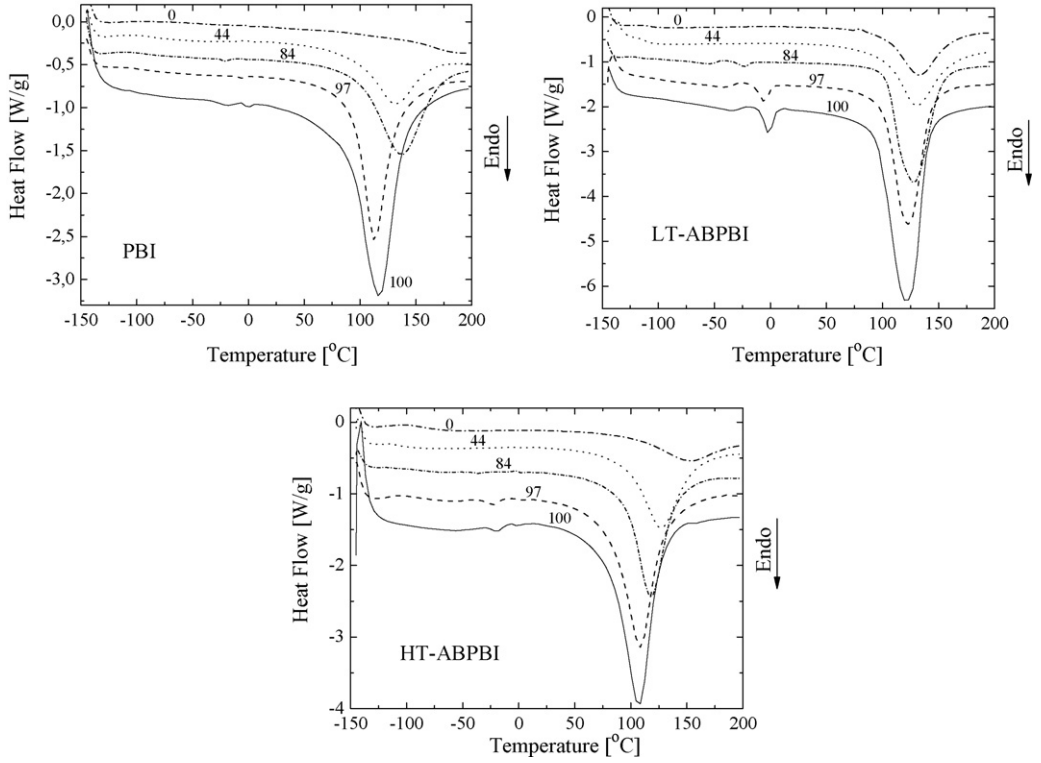

Fig. 2. DSC curves of PBI, LT-ABPBI, HT-ABPBI membranes equilibrated at different % RH (indicated on the curves). Scan rate: 10 °C min^{-1}.

in Fig. 2. The intensity of these peaks increased as increasing RH. According to the values reported in Table 2, the water content in the membranes follows the order LT-ABPBI > HT-ABPBI > PBI, which is also the order of the relative intensity of the peaks for the three membranes compared at the same RH.

The desorption temperature shifted to higher temperatures with decreasing RH, the effect being more pronounced for the HT-ABPBI membrane. The shift is an indication that as lower is the amount of water in the system, the stronger is its interaction with the protonated imidazol groups and the formation of hydrogen bonds with the phosphoric acid.

The LT-ABPBI sample equilibrated at 0% RH still retained a considerable amount of water as can be observed through the presence of the water desorption peak above 100 °C. On the contrary, PBI had lost most of the water through exposure at 0% RH. The difference could be related to the presence of less water per mol of phosphoric acid in PBI, as indicated by the parameter λ_{wa} in Table 1. As expected from the similar value of λ_{wa}, the behavior of water desorption behavior for HT-ABPBI at 0% RH is closer to PBI.

3.1.2. Glass transition

The very low temperature region ($-140\,^{\circ}C < T < -70\,^{\circ}C$) of the DSC thermograms corresponding to PBI and ABPBI (LT and HT) acid-doped membranes are magnified in Fig. 3 (note the differences in the *y*-axis scale), where the signature of a glass transition can be observed in most of the scans. The glass transition temperatures and the corresponding heat capacity changes at T_g are summarized in Table 3. The values ranged from $-73\,^{\circ}C$ to $-120\,^{\circ}C$ for all the membranes over the entire range of RH.

For the LT-ABPBI membrane, the glass transition was too weak to be detected in the samples at 97% RH, but the thermogram showed a baseline deviation close to $-102\,^{\circ}C$.

In order to understand the nature of the observed glass transition in the ternary system (water + phosphoric acid + polymer) it is important to summarize our knowledge on the glass transitions of the pure polymer system and of the binary H_3PO_4–H_2O mixtures.

The glass transition of PBI has been studied by several authors [44–47]. Chung and Chen [44] measured $T_g = 415\,^{\circ}C$ for PBI using DMA. Menczel [45] observed T_g ranging from 387 °C to 465 °C, when DSC and DMA techniques were used. Földes et al. [46] measured the glass transition of pure PBI and blends with other polymer using TMA ($T_g = 390\,^{\circ}C$) and DSC ($T_g = 370\,^{\circ}C$). More recently, Zaidi [47] reported $T_g = 398\,^{\circ}C$ for PBI using DSC. The observed differences in these reported glass transition temperatures are in part due to the employed experimental technique and probably to the different molecular weight of the PBI samples, although the mean T_g value is around 400 °C.

On the other hand, no glass transition temperature has been reported for neither, pristine ABPBI, nor H_3PO_4-doped PBI and ABPBI membranes. While for ABPBI T_g is expected to be closer to that of PBI, the high content of H_3PO_4 in the acid-doped membranes should lead to a decrease of the glass transition temperature due to a plastifying effect.

Recently, we determined the glass transition temperatures of aqueous solutions of H_3PO_4 and found that their composition dependence obeys the Taylor–Gordon equation [48]:

$$T_g = \frac{w_2 T_{g2} + w_1 k T_{g1}}{w_2 + w_1 k} \quad (1)$$

where w_1 and w_2 are the weight fraction of water and H_3PO_4, respectively; $T_{g1} = -137\,^{\circ}C$ and $T_{g2} = -82.8\,^{\circ}C$ are the glass transition temperature of water and H_3PO_4, respectively, and k is the empirical (best fit) coefficient which was found to be 2.76.

The calculated glass transition temperature of a 68.8 wt% (10.64 M) H_3PO_4 aqueous solution is $-111\,^{\circ}C$, according to Eq. (1), and it shifts to lower temperatures with increasing water content, reaching a value of $-120\,^{\circ}C$ close to 50 wt%. It is expected that H_3PO_4 confined into the membrane aqueous domains could exhibit different T_g values, although maintaining the same trend with the water content.

The values of T_g reported in Table 3 can be interpreted taking into account the supplemented phase diagram of the H_3PO_4–H_2O system [49] shown in Fig. 4, where the glass transition of the aqueous acid is shown, besides the equilibrium transitions involving water, orthophosphoric acid (H_3PO_4), and orthophosphoric acid hemi-hydrate ($2H_3PO_4{\cdot}H_2O$).

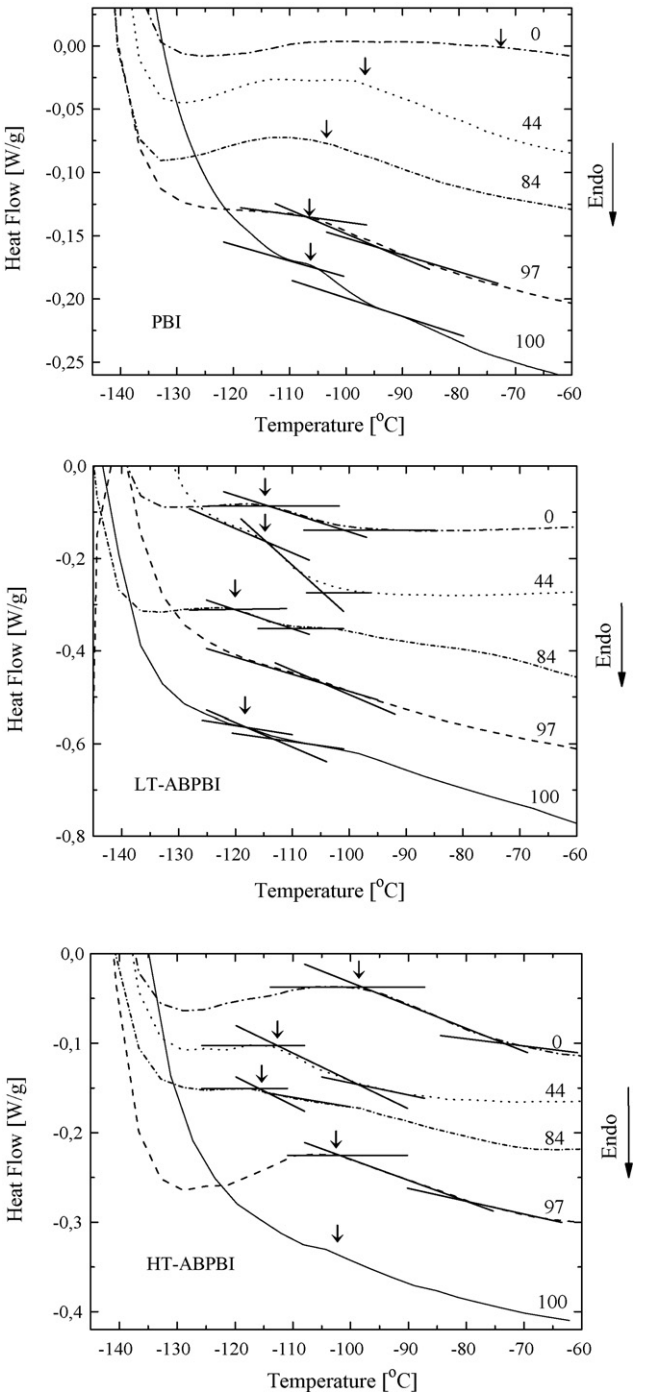

Fig. 3. Magnification of the DSC thermograms of Fig. 2 at different % RH (indicated on the curves) in the very low temperature region. The onset of the glass transition is indicated by an arrow in all the curves.

Table 3
Glass transition temperature (T_g), reversible change of specific heat capacity at T_g (ΔC_p), water crystallization and melting temperatures (T_c and T_m, respectively), heats of crystallization (ΔH_c) and fusion (ΔH_f) per gram of sample, and the percentage of frozen water content (W_f^T) in PBI and ABPBI, at different RH values.

Water%RH	Membrane	T_g (°C)	ΔC_p (J g^{-1} K^{-1})	T_c (°C)	T_m (°C)	ΔH_c (J g^{-1})	ΔH_m (J g^{-1})	ΔH_c^f (J g^{-1}) (free water)	ΔH_m^f (J g^{-1}) (free water)	W_f^T (%)
0	PBI	−73	0.22	–	–	–	–	0.10	−0.088	–
	LT-ABPBI	−115	0.43	–	–	–	–	–	–	–
	HT-ABPBI ABPBIHigh	−97	0.58	–	–	–	–	–	–	–
44	PBI	−96	0.27	–	–	–	–	0.22	−0.19	0.2
	LT-ABPBI	−115	0.73	–	–	–	–	–	–	0
	HT-ABPBI ABPBIHigh	−112	0.34	–	–	–	–	0.13	−0.17	0.1
84	PBI	−102	0.24	−27	−20	0.081	−0.83	0.020	−0.039	0.7
	LT-ABPBI	−120	0.27	−43	−23	3.5	−5.64	–	–	2.5
	HT-ABPBI ABPBIHigh	−108	0.35	−50	−36	0.36	−0.78	0.20	−0.27	0.5
97	PBI	−104	0.24	−13	−8	0.16	−0.57	–	–	0.4
	LT-ABPBI	–	–	−26	−5	10	−16.2	–	–	6.5
	HT-ABPBI ABPBIHigh	−102	0.43	−41	−22	1.3	−3.37	0.14	−0.26	1.5
100	PBI	−107	0.23	−38	−19	1.3	−1.92	0.23	−1.62	2.2
	LT-ABPBI	−118	–	−18	−2	–	–	11.1	−23	9.1
	HT-ABPBI ABPBIHigh	−112	–	−30	−18	1.6	−2.21	0.38	−0.48	1.1

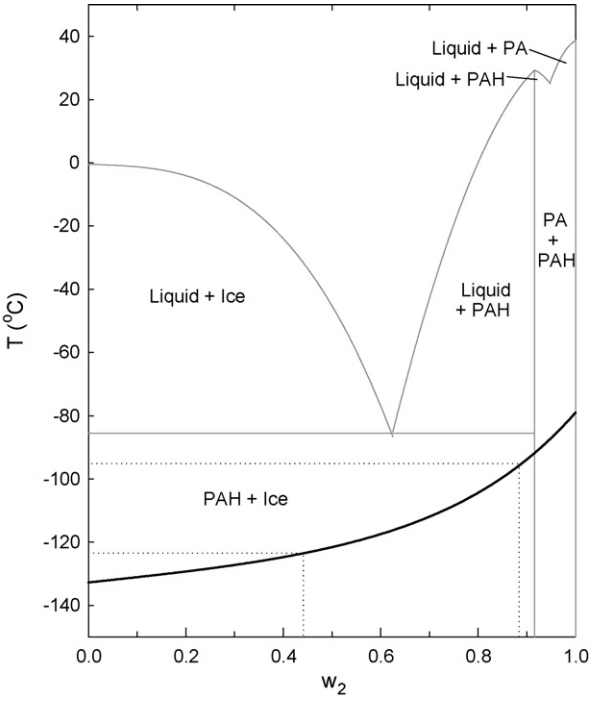

Fig. 4. Supplemented phase diagram of the system phosphoric acid–water, showing the coexistence of liquid–solid and solid–solid phases (PA: orthophosphoric acid (H_3PO_4); PAH: orthophosphoric acid hemi-hydrate ($2H_3PO_4{\cdot}H_2O$)) adapted from the known phase diagram [49]. The solid line is the best fit of the T_g of the acid solutions extrapolated to the glass transition of pure water (−137 °C).

The mass fractions of H_3PO_4 in the membranes as a function of the RH are shown in Table 2, and can be converted to mass fraction of the binary H_3PO_4–H_2O mixture in the membrane. Thus, the binary mass fraction of H_3PO_4 when the RH decreased from 100 to 32% ranged from 0.48 to 0.85 for LT-ABPBI, from 0.44 to 0.88 for HT-ABPBI, and from 0.58 to 0.82 for PBI. If we assume that the observed T_g corresponds to the glass transition of the H_3PO_4–H_2O mixture, the expected glass transition will be in the range $-125\,^{\circ}C < T_g < -90\,^{\circ}C$, as indicated in Fig. 4, in good agreement with the measured values. This approach discards any effect of the polymeric matrix on the observed transition temperature, and the glass transition temperatures of the systems are consequently assumed to correspond to the T_g values of aqueous H_3PO_4.

A rough idea of the effect of the polymer matrix on T_g can be assessed by assuming the ternary polymer–H_3PO_4–H_2O as a pseudo binary system polymer-(H_3PO_4–H_2O) and resorting to the Fox equation (Eq. (2)), which was used successfully to describe the T_g of blends of PBI with other polymers [46]:

$$\frac{1}{T_g} = \frac{1}{T_{g1}} + \frac{1}{T_{g2}} \tag{2}$$

The calculated values of T_g are between −107 °C and −38 °C, assuming that the polymer mass fraction of the mixtures ranged from $0.14 < w_2 < 0.38$ (calculated from the water and acid uptake by the membranes), and the corresponding glass transition temperatures for pure PBI or ABPBI is $T_{g2} \approx 400\,^{\circ}C$, while for the mixture of aqueous phosphoric acid: $-125\,^{\circ}C < T_{g1} < -83\,^{\circ}C$. As expected, these estimated T_g values are much closer to the T_g of the aqueous acid than to the T_g values of the polymer, reflecting weak polymer–water or polymer–aqueous acid solution interactions, which determine that the acid solution governs the T_g values of the system. Although the upper limit of the estimated T_g is much higher than that measured, the agreement can be considered satisfactory, taking into account the simplicity of the approach.

Finally, an alternative explanation to the observed thermal relaxation in this low temperature region is possible, having into account that, in addition to the primary (α) relaxation, a low temperature (δ) relaxation was detected by DMA in PBI samples at −90 °C [45]. This low temperature relaxation, not observed in the DSC study, was assigned to the onset of rotation of the m-phenylene ring. One could speculate on the possibility that the presence of phosphoric acid and water in the polymer enhances this relaxation and causes the transitions to be observable by DSC. This hypothesis would require a more detailed analysis, using other techniques, which is out of the scope of this work.

It is worthy to discuss briefly the possibility that the low temperature relaxations correspond to the melting of the eutectic H_3PO_4–H_2O mixture segregated during the cooling step. At high RH (≥84%) the H_3PO_4–H_2O mixtures have compositions located on the water-rich region of the phase diagram meaning that ice could separate upon cooling, and a solid with the eutectic composition ($w_2 \approx 0.62$) would segregate at around −85 °C. The eutectic temperature of the confined H_3PO_4–H_2O mixtures could change in relation to the binary system and one would be tempted to assign the observed transition to the melting of the eutectic mixture upon warming. However, as will be discussed below, the small amount of ice observed in the DSC scans, compared to the ice segregation

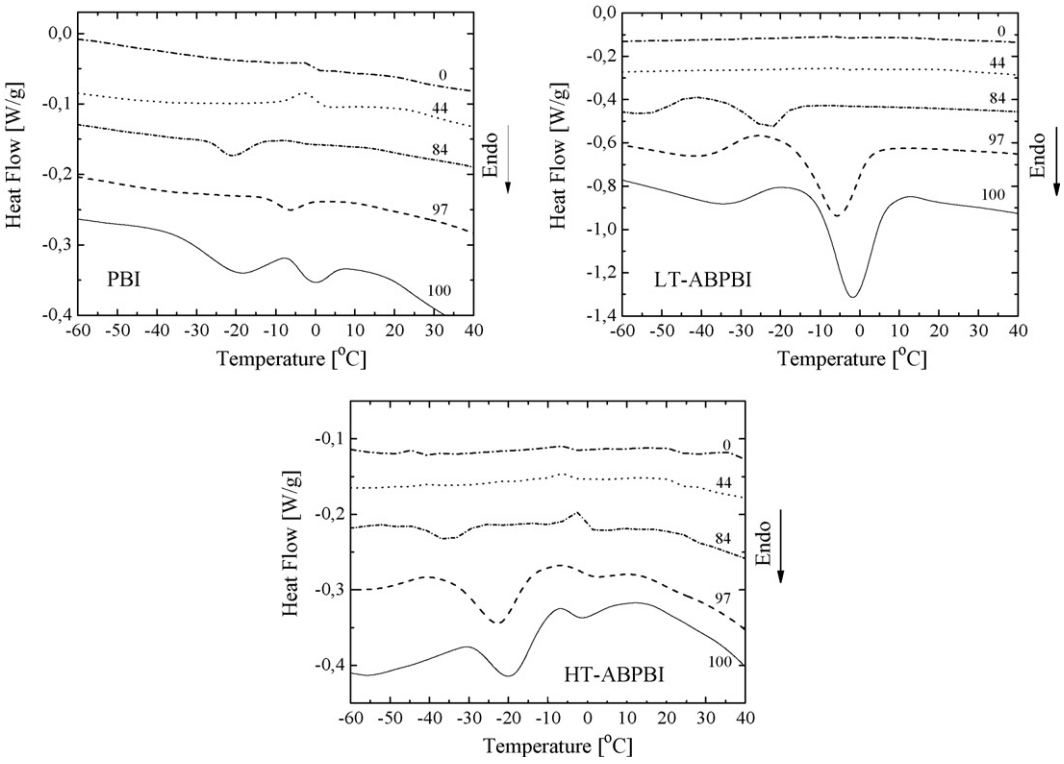

Fig. 5. Magnification of the DSC thermograms of Fig. 2 at different % RH (indicated on the curves) in the region of water crystallization/melting.

needed to reach the eutectic composition, would indicate that this explanation is not very plausible.

3.1.3. Water crystallization and melting

There are several generic features, with respect to the behavior of water, that are common to a wide variety of hydrated polymeric system [50]. To the extent of this work it will be enough to consider that strongly hydrated membranes (>84% RH) may contain water of three different types associated with them, which can be characterized by DSC measurements: (1) water that remains unfrozen upon cooling to −146 °C, due to its strong interactions with the polymer matrix, enhanced by the presence of phosphoric acid molecules, (2) water that displays weak interactions with the polymer matrix and can be frozen upon cooling to −146 °C, and (3) free water that behaves like bulk water since does not interact intimately with the polymer chain.

The intermediate regions of the DSC scans, in the temperature range $-70\,^{\circ}C < T < 40\,^{\circ}C$, in Fig. 2 indicate the presence of weak endothermic peaks, which are magnified in Fig. 5. They can be attributed to the melting of previously frozen water. In strongly hydrated PBI, LT-ABPBI and HT-ABPBI membranes (≥84% RH), endothermic peaks corresponding to the melting of frozen water were present, and they shifted to higher temperatures with increasing relative humidity, approaching 0 °C, the melting temperature of bulk water. This is well illustrated in Fig. 5 for LT-ABPBI at 100% RH, because of the high water content in this system.

The shift to higher temperatures with increasing relative humidity, supports the assumption that these endothermic peaks are due to water melting. The depression of melting temperatures in comparison with the value for bulk water can be explained by the interaction of water with polymer matrix and phosphoric acid molecules [51].

In HT-ABPBI and PBI membranes, endothermic peaks associated to the melting of frozen bulk-like water were also observed around 0 °C, regardless of the relative humidity of the membranes.

Almost all of the endothermic peaks in Fig. 5 have adjacent exothermic peaks associated, with onset temperatures from −61 °C to −4 °C, which can be attributed to the crystallization of water that remained supercooled during cooling at −145 °C and was allowed to crystallize during the DSC run.

The endothermic peaks in the DSC curves are attributed to the water that can be readily frozen and the frozen water content of ABPBI and PBI membranes can be estimated from the areas of those peaks. The value of the melting enthalpy of ice I, 333.8 J g^{-1}, was employed to estimate the frozen water content. The percentage of the total frozen water (W_f^T), was then obtained relative to the total water content, and depicted in Table 3.

Both ABPBI and PBI membranes presented a low percentage of frozen water (<10 wt% of the total water content). PBI and HT-ABPBI membranes exhibited very low values of frozen water, while for the LT-ABPBI membrane the quantity of frozen water was considerably higher, with a maximum of 9.1 wt% at 100% RH, which is consistent with its higher water uptake.

3.2. Low temperature DSC scans of ABPBI and PBI equilibrated with water–methanol

The DSC thermograms of the doped membranes equilibrated in different methanol–water solutions are presented in Fig. 6 (note the differences in the *y*-axis scale). The thermograms for the samples with 0 wt% of methanol are identical to those shown in Fig. 2 for 100% RH. In Table 4, the characteristic heats and temperatures of the thermograms, and the percentange of frozen water are depicted.

The presence of two types of frozen water was also manifested in the membranes equilibrated in methanol–water solutions, as indicated by the melting temperature ranges: one population of frozen water with lower melting temperatures, manifesting high interactions with the polymer, and bulk-like water, with melting characteristics close to those of pure water, as described before. The first type of water molecules was observed in samples from

Table 4
Water crystallization and melting temperatures (T_c and T_m, respectively), heats of crystallization (ΔH_c) and fusion (ΔH_f), and the percentage of frozen water content (W_f^T) in PBI and ABPBI samples equilibrated in methanol–water solutions of different compositions.

CH_3OH (wt%)	Membrane	T_c (°C)	T_m (°C)	ΔH_c (J g^{-1})	ΔH_m (J g^{-1})	N (g g^{-1}) (dry)	W_f^T (%)
25	PBI	−24	−9	4.0	−14	0.69	10.3
	LT-ABPBI	−31	−12	3.4	−10	2.35	4.3
	HT-ABPBI	−42	−26	0.61	−1.3	2.25	0.6
50	PBI	−30	−18	3.6	−6.5	0.46	6.2
	LT-ABPBI	−39	−21	2.6	−2.6	1.57	1.3
	HT-ABPBI	−8	−5	0.32	−0.30	1.50	0.1
75	PBI	−4	−3	0.054	−0.12	0.23	0.2
	LT-ABPBI	−2	−1	0.21	−0.20	0.78	0.1
	HT-ABPBI	−2	1	0.51	−0.55	0.75	0.4
100	PBI	−4	−2	0.69	−0.43	–	–
	LT-ABPBI	−9	−4	0.43	−0.26	–	–
	HT-ABPBI	−5	−3	0.55	−0.14	–	–

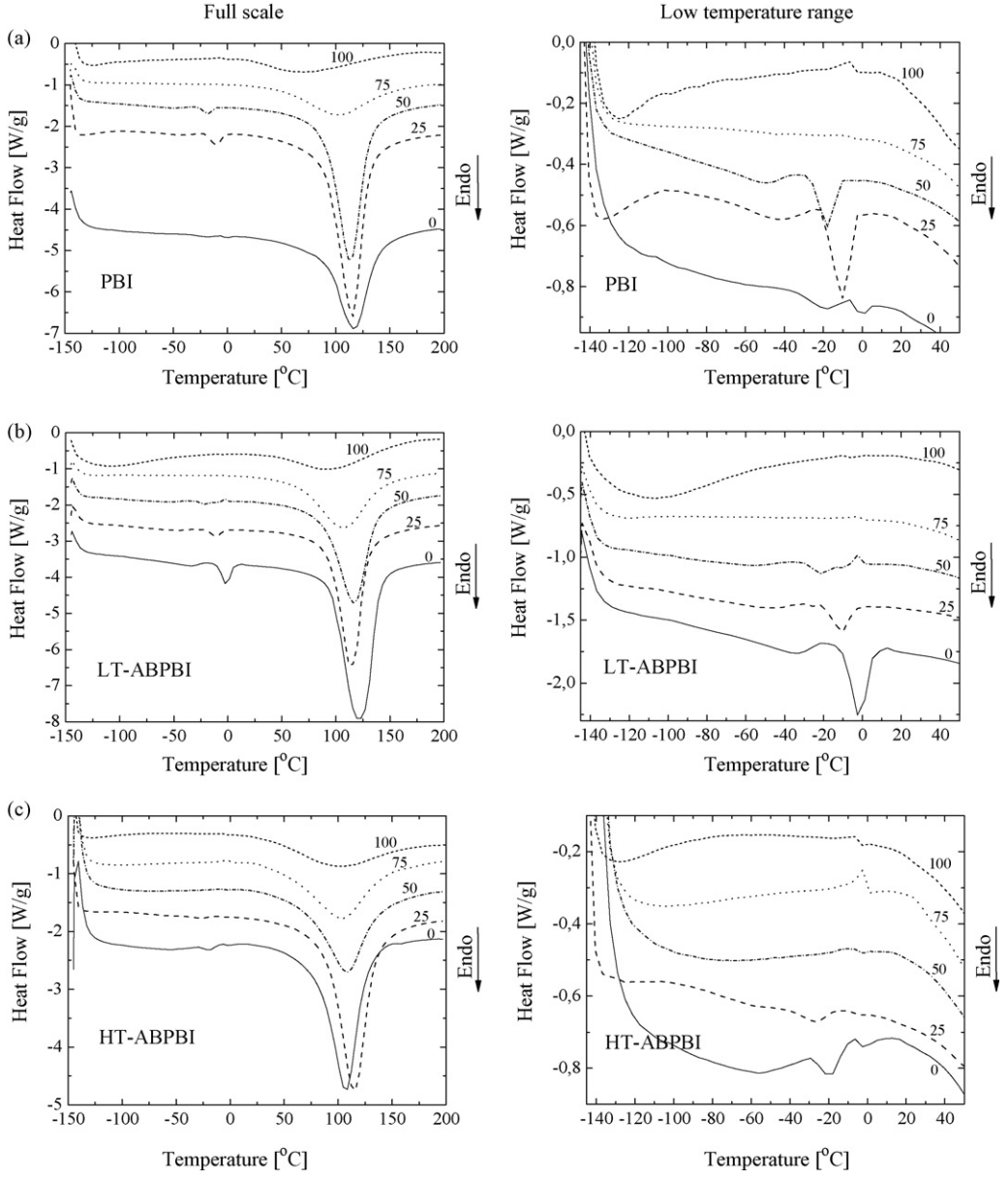

Fig. 6. DSC curves of the PBI, LT-ABPBI, and HT-ABPBI membranes equilibrated in methanol–water solutions. The numbers indicate the wt% of methanol in the mixture. Scan rate: 10 °C min^{-1}.

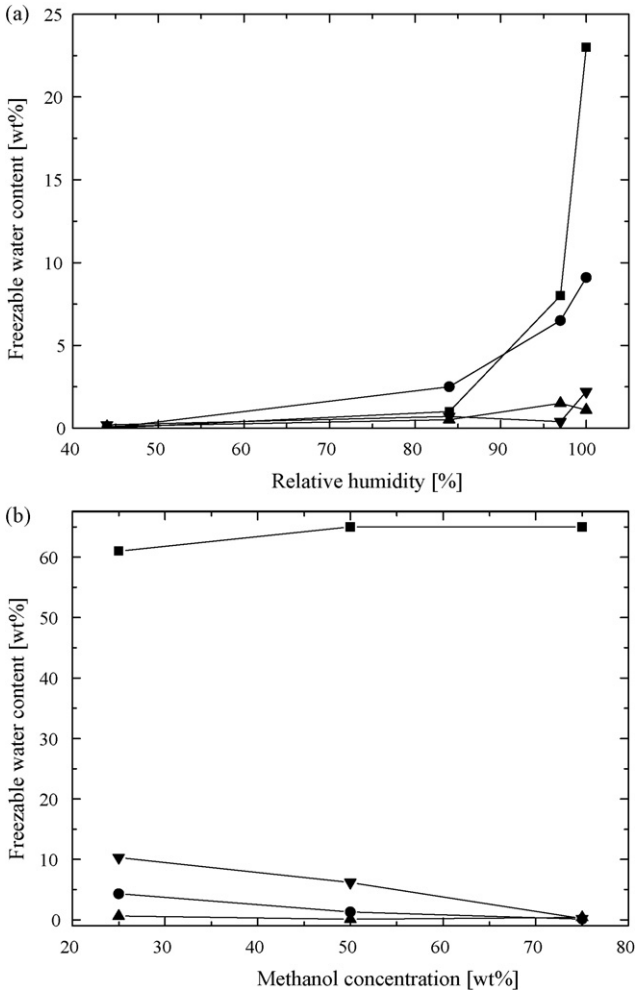

Fig. 7. Percentage of frozen water after cooling up to −146 °C, in LT-ABPBI (●), HT-ABPBI (▲), PBI (▼) and Nafion® (■) [40]. (a) Membranes equilibrated in water as a function of relative humidity in the membranes and (b) membranes equilibrated in water–methanol as a function of methanol concentration.

0 to 50 wt% methanol in LT-ABPBI and PBI, and from 0 to 25 wt% methanol in HT-ABPBI. Melting peaks shifted slightly towards lower temperatures as the methanol concentration increased from 0 to 50 wt% methanol, in agreement with previous result for Nafion® membranes in methanol–water solutions [40].

The melting of small quantities of bulk-like frozen water was also observed in all membranes for methanol concentrations ≥ 75 wt%. That means that the acid-doped membranes retain small quantities of water, through hydrogen bonding and electrostatic interactions with the protonated imidazole groups, even when equilibrated in pure liquid methanol.

For PBI membranes in water–methanol, water crystallization and melting peak areas were larger than those obtained for the samples equilibrated in pure water. In order to estimate the amount of frozen water, the solubility of water in the samples at the different water–methanol compositions were calculated assuming that the composition in the membrane was identical to that of the binary liquid mixture where it was immersed.

As expected, in all cases the percentage of frozen water decreased with increasing amount of methanol in the membrane. For PBI in methanol–water solutions with methanol wt% ≥ 50%, the percentage of frozen water was much larger than the corresponding to PBI membranes in pure water (2.2 wt%). Conversely, in ABPBI the amount of frozen water was lower in the case of the samples equilibrated in methanol–water solutions than for those equilibrated in pure water at different RH.

3.3. Frozen water in the PBI, ABPBI and Nafion® membranes

The amount of frozen water as a function of relative humidity is shown in Fig. 7a for ABPBI, PBI and Nafion® membranes. When compared to Nafion®, the widely used membrane in PEM and DM PEM fuel cells, ABPBI and PBI membranes presented a small quantity of frozen water, 1.5–9 wt% against 23 wt% for Nafion® at 100% RH.

In Fig. 7b, the results presented in Section 3.2 for the membranes equilibrated with methanol solutions were compared to those reported for Nafion® [40]. Nafion® presents a much higher content of frozen water, after cooling to −146 °C, as in the case of present samples, than both, ABPBI and PBI membranes. Frozen water in Nafion® membranes was almost independent of methanol compositions, with values as high as 61–65 wt%, while PBI membranes exhibit a maximum of 10 wt% of frozen water. ABPBI membranes, particularly HT-ABPBI presented very low percentages of frozen water in all methanol concentrations studied, with a maximum value of 0.6 wt% at 25 wt% methanol.

This result is relevant for the application of ABPBI in DM PEM fuel cells because it means that the electrical conductivity of the electrolyte membranes will be slightly reduced by the reduction of water content due to freezing and, consequently, the fuel cell start up at low temperatures will not be affected.

In ABPBI and PBI samples immersed in methanol–water solutions no thermal relaxation attributable to a glass transition seemed to occur below −70 °C. However, desorption peaks were also observed for these membranes in the thermograms of Fig. 6, with onset temperatures higher than 80 °C. Desorption temperatures decreased with increasing methanol content in the samples, coincidently with the lower boiling temperature of methanol with respect to water.

4. Conclusions

A comprehensive analysis of the thermal properties of PBI and ABPBI membranes on a wide range of temperature was performed for samples equilibrated in vapor water and in liquid water–methanol mixtures. Three different regions of the thermograms were discussed in relation to glass transition, water crystallization/melting and water or water/methanol desorption.

The thermal relaxation observed in the very low temperature region seems to be related to the glass transition of the H_3PO_4–H_2O mixture inside the polymer matrix, although affected by the presence of strong interaction of the imidazole groups with both components. Other alternative explanation for the weak relaxations is also discussed in Section 3.1, although they seem to be less plausible. The low temperature relaxations in PBI membranes prepared via sol–gel process [18] are expected to shift to lower temperatures due to they higher content of phosphoric acid.

The desorption of water in the high temperature region can be easily interpreted in terms of its interactions with phosphoric acid and the polymer as a function of the water content (determined by the RH). The thermal events occurring close to 0 °C and at subzero temperatures are important to determine the amount of frozen water in the membranes. The obtained results confirm that ABPBI and PBI membranes are good electrolyte candidates in PEM, and particularly DM PEM, fuel cells in a wide temperature range. At temperatures below 0 °C, water in the membrane may crystallize affecting ionic conduction, concerning mainly the start up procedure. Although conductivities of doped ABPBI and PBI at low

temperatures are low, the fact they present almost no frozen water is an advantage, of major significance in relation to the applicability of fuel cells in cold environments.

Acknowledgments

The authors thank financial support from Agencia Nacional de Promoción Científica y Tecnológica (PICT Start Up 35403 and PAE 36985) and CNEA. HRC and MPB are members of the Consejo Nacional de Investigaciones Científicas y Técnicas (CONICET). FNP thanks doctoral fellowships from CNEA and CONICET.

References

[1] J.S. Wainright, J.-T. Wang, D. Weng, R.F. Savinell, M. Litt, J. Electrochem. Soc. 142 (1995) L121–L123.
[2] K.D. Kreuer, J. Membr. Sci. 185 (2001) 29–39.
[3] J.A. Kerres, J. Membr. Sci. 185 (2001) 3–27.
[4] M. Rikukawa, K. Sanui, Prog. Polym. Sci. 25 (2000) 1463–1502.
[5] L. Carrette, K.A. Friedrich, U. Stimming, Chem. Phys. Chem. 1 (2000) 162–193.
[6] K.D. Kreuer, Chem. Phys. Chem. 3 (2002) 771–775.
[7] M.F.H. Schuster, W.H. Meyer, M. Schuster, K.D. Kreuer, Chem. Mater. 16 (2004) 329–337.
[8] Q. Li, R. He, J.O. Jensen, N.J. Bjerrum, Chem. Mater. 15 (2003) 4896–4915.
[9] K.D. Kreuer, S.J. Paddison, E. Spohr, M. Schuster, Chem. Rev. 104 (2004) 4637–4678.
[10] Q. Li, J.O. Jensen, R.F. Savinell, N.J. Bjerrum, Prog. Polym. Sci. 34 (2009) 449–477.
[11] A. Buckley, D.E. Stuetz, G.A. Serad, in: H.F. Mark, N.M. Bikales, C.G. Overberger, G. Menges (Eds.), Encyclopedia of Polymer Science and Engineering, vol. 11, Wiley–Interscience, New York, 1988, pp. 572–601.
[12] M.F.H. Schuster, W.H. Meyer, Annu. Rev. Mater. Res. 33 (2003) 233–261.
[13] S.R. Samms, S. Wasmus, R.F. Savinell, J. Electrochem. Soc. 143 (1996) 1225–1232.
[14] Y.L. Ma, J.S. Wainright, M.H. Litt, R.F. Savinell, J. Electrochem. Soc. 151 (2004) A8–A16.
[15] R.F. Savinell, E. Yeager, D. Tryk, U. Landau, J. Wainright, D. Weng, K. Lux, M. Litt, C. Rogers, J. Electrochem. Soc. 141 (1994) L46–L48.
[16] R. Bouchet, E. Siebert, Solid State Ionics 118 (1999) 287–299.
[17] M. Kawahara, J. Morita, M. Rikukawa, K. Sanui, N. Ogata, Electrochim. Acta 45 (2000) 1395–1398.
[18] L. Xiao, H. Zhang, E. Scanlon, L.S. Ramanathan, E.W. Choe, D. Rogers, T. Apple, B.C. Benicewicz, Chem. Mater. 17 (2005) 5328–5333.
[19] Q. Li, R. He, J.O. Jensen, N.J. Bjerrum, Fuel Cells 4 (2004) 147–159.
[20] Q. Li, R. He, R.W. Berg, H.A. Hjuler, N.J. Bjerrum, Solid State Ionics 168 (2004) 177–185.
[21] J.–T. Wang, R.F. Savinell, J. Wainright, M. Litt, H. Yu, Electrochim. Acta 41 (1996) 193–197.
[22] C. Wannek, W. Lehnert, J. Mergel, J. Power Sources 192 (2009) 258–266.
[23] M.J. Ariza, D.J. Jones, J. Rozière, Desalination 147 (2002) 183–189.
[24] J.A. Asensio, S. Borrós, P. Gómez-Romero, Electrochim. Acta 49 (2004) 4461–4466.
[25] J. Jouanneau, R. Mercier, L. Gonon, G. Gebel, Macromolecules 40 (2007) 983–990.
[26] J.A. Asensio, S. Borrós, P. Gómez-Romero, J. Polym. Sci. (A): Polym. Chem. 40 (2002) 3703–3710.
[27] A. Carollo, E. Quartarone, C. Tomasi, P. Mustarelli, F. Belotti, A. Magistris, F. Maestroni, M. Parachini, L. Garlaschelli, P.P. Righetti, J. Power Sources 160 (2006) 175–180.
[28] J.A. Asensio, P. Gómez-Romero, Fuel Cells 5 (2005) 336–343.
[29] M.K. Daletou, N. Gourdoupi, J.K. Kallitsis, J. Membr. Sci. 252 (2005) 115–122.
[30] L. Xiao, H. Zhang, T. Jana, E. Scanlon, R. Chen, E.W. Choe, L.S. Ramanathan, S. Yu, B.C. Benicewicz, Fuel Cells 5 (2005) 287–295.
[31] H. Pu, Q. Liu, G. Liu, J. Membr. Sci. 241 (2004) 169–175.
[32] L.A. Diaz, G.C. Abuin, H.R. Corti, J. Power Sources 188 (2009) 45–50.
[33] E.A. Franceschini, H.R. Corti, J. Power Sources 188 (2009) 379–386.
[34] L.R. Belohlav, Angew. Makromol. Chem. 40 (1974) 465–483.
[35] M. Jaffe, M.I. Haider, J. Menczel, J. Rafalko, Polym. Eng. Sci. 32 (1992) 1236–1241.
[36] T.K. Ahn, M. Kim, S. Choe, Macromolecules 30 (1997) 3369–3374.
[37] C.E. Hughes, S. Haufe, B. Angerstein, R. Kalim, U. Mahr, A. Reiche, M. Baldus, J. Phys. Chem. B 108 (2004) 13626–13631.
[38] J.A. Asensio, S. Borros, P. Gomez-Romero, J. Electrochem. Soc. 151 (2004) A304–A310.
[39] D.W. Tomlin, A.V. Fratini, M. Hunsaker, W. Wade Adams, Polymer 41 (2000) 9003–9010.
[40] H.R. Corti, F. Nores-Pondal, M.P. Buera, J. Power Sources 161 (2006) 799–805.
[41] R.B. Anderson, J. Am. Chem. Soc. 68 (1946) 686–691.
[42] J.H. de Boer, The Dynamical Character of Adsorption, Clarendon Press, Oxford, 1953.
[43] E.A. Guggenheim, Applications of Statistical Mechanics, Clarendon Press, Oxford, 1966.
[44] T.S. Chung, P.N. Chen, Polym. Eng. Sci. 30 (1990) 1–7.
[45] J.D. Menczel, J. Therm. Anal. Calorim. 59 (2000) 1023–1027.
[46] E. Földes, E. Fekete, F.E. Karasz, B. Pukánszky, Polymer 41 (2000) 975–983.
[47] S.M.J. Zaidi, Electrochim. Acta 50 (2005) 4771–4777.
[48] H.R. Corti, F. Nores-Pondal, unpublished results.
[49] Kirk-Othmer Encyclopedia of Chemical Technology, vol. 17, 3rd edition, John Wiley & Sons, 1982, p. 433.
[50] V.J. McBrierty, S.J. Martin, F.E. Karasz, J. Mol. Liq. 80 (1999) 179–205.
[51] K. Asaka, N. Fujiwara, K. Oguro, K. Onishi, S. Sewa, J. Electroanal. Chem. 505 (2001) 24–32.